Published in final edited form as:

Mol Cancer Ther. 2021 November ; 20(11): 2291–2301. doi:10.1158/1535-7163.MCT-21-0109.

Cytotoxic Engineered Induced Neural Stem Cells as an Intravenous Therapy for Primary Non-Small Cell Lung Cancer and Triple-Negative Breast Cancer

Alison R. Mercer-Smith[1,*], **Wulin Jiang**[1,*], **Juli R. Bago**[2], **Alain Valdivia**[1], **Morrent Thang**[1], **Alex S. Woodell**[1], **Stephanie A. Montgomery**[3], **Kevin T. Sheets**[1], **Carey K. Anders**[4], **Shawn D. Hingtgen**[1,5]

[1]Division of Pharmacoengineering and Molecular Pharmaceutics, UNC Eshelman School of Pharmacy, The University of North Carolina at Chapel Hill, Chapel Hill, North Carolina, 27599-USA

[2]Department of Hemato-Oncology, University of Ostrava, Czech Republic

[3]Pathology and Laboratory Medicine, The University of North Carolina at Chapel Hill, Chapel Hill, North Carolina, 27599-USA

[4]Department of Medicine, Duke University, North Carolina, 27710-USA

[5]Department of Neurosurgery, The University of North Carolina at Chapel Hill, Chapel Hill, North Carolina, 27599-USA

Abstract

Converting human fibroblasts into personalized induced neural stem cells (hiNSCs) that actively seek out tumors and deliver cytotoxic agents is a promising approach for treating cancer. Herein, we provide the first evidence that intravenously-infused hiNSCs secreting cytotoxic agent home to and suppress the growth of non-small cell lung cancer (NSCLC) and triple negative breast cancer (TNBC). Migration of hiNSCs to NSCLC and TNBC *in vitro* was investigated using time-lapse motion analysis, which showed directional movement of hiNSCs to both tumor cell lines. *In vivo*, migration of intravenous hiNSCs to orthotopic NSCLC or TNBC tumors was determined using bioluminescent imaging (BLI) and immunofluorescent post-mortem tissue analysis, which indicated that hiNSCs co-localized with tumors within 3 days of intravenous administration and persisted through 14 days. *In vitro*, efficacy of hiNSCs releasing cytotoxic TRAIL (hiNSC-TRAIL) was monitored using kinetic imaging of co-cultures, in which hiNSC-TRAIL therapy induced rapid killing of both NSCLC and TNBC. Efficacy was determined *in vivo* by infusing hiNSC-TRAIL or control cells intravenously into mice bearing orthotopic NSCLC or TNBC and tracking changes in tumor volume using BLI. Mice treated with intravenous hiNSC-TRAIL showed a 70 or 72% reduction in NSCLC or TNBC tumor volume compared to controls within 14 or 21 days, respectively. Safety was assessed by hematology, blood chemistry, and histology, and no significant changes in these safety parameters was observed through 28 days. These results

Contact information: Shawn Hingtgen, 4212 Marsico Hall, 120 Mason Farm Road, Chapel Hill, NC 27599, 919-537-3827, hingtgen@email.unc.edu.

*Authors contributed equally

indicate that intravenous hiNSCs-TRAIL seek out and kill NSCLC and TNBC tumors, suggesting a potential new strategy for treating aggressive peripheral cancers.

Keywords

Cell-based therapy; induced neural stem cells; systemic infusion; non-small cell lung cancer; triple-negative breast cancer

INTRODUCTION

Lung and breast cancer are the most common forms of cancer in the United States, together accounting for an estimated 29% of all new cancer cases diagnosed in 2018; these cancers are among the deadliest, accounting for nearly 1/3 of all cancer deaths (1). There remains a significant need for more effective systemic treatments to improve the care for patients suffering from these cancers. Emerging data suggests cell therapies may represent a novel and effective new treatment option.

Neural stem cells (NSCs) have emerged as promising anti-cancer drug delivery vehicles due to their innate tumor tropism (2–7). Several studies have shown genetically engineered NSCs home selectively to brain cancer, allowing them to deliver anti-cancer gene products directly to local and distant tumor foci, significantly reducing tumor volumes and markedly extending survival (2, 7–10). Not limited to the brain, new studies have demonstrated that intravenously-infused tumoricidal NSCs extravasate from vessels to populate tumor foci and significantly reduce human cancer in orthotopic mouse models of breast cancer, lung cancer, and a variety of other tumor types (2, 5–11). These studies demonstrate the potential of tumor-homing NSC therapy for the treatment of aggressive extracranial cancers; as these treatments move forward, the ideal source of NSCs remains in question.

Selecting the most effective NSC carrier will be critical to maximizing persistence, tumor targeting, and ultimately tumor kill in human patient trials. Allogeneic NSCs have shown success in preclinical testing (8, 11–14) and safety in early-stage human clinical trials for gliomas (2, 9, 15). However, the high potential of allogeneic stem cell transplants for immune-mediated rejection (16) is likely to limit their residence time at tumors and ability to deliver therapeutic agents directly to peripheral cancer foci. In contrast, personalized NSC therapy holds the potential to avoid rapid immune clearance (16). This holds the potential to maximize treatment response in patients by increasing the cell carriers that reach tumor foci, increasing cell carrier residence time, and delivering a more durable exposure for the therapeutic window to induce tumor kill. We recently discovered that transdifferentiation, a process that directly converts somatic cells into other adult cell types, can be used to generate tumor-homing drug carriers that regress tumor xenografts, known as human induced NSC (hiNSC) (17, 18). Using SOX2 as a single transcriptional factor, we transformed human fibroblasts into hiNSCs within one week of culture (17); we have shown this process is effective in transdifferentiating patient fibroblasts to be used in the treatment of patient-derived intracranial tumors (19). While the fibroblasts show random movement, the hiNSCs following transdifferentiation show significant directional migration to a tumor (17). The hiNSCs express NSC markers SOX2 and Nestin and the neuronal

marker TUJ-1 with minimal expression of the astrocyte marker GFAP or pluripotency markers NANOG or OCT4 (17). *In vivo*, hiNSCs maintained expression of the NSC marker Nestin while expression of neuronal markers or pluripotency markers was virtually absent (17, 19). In the clinic, hiNSC therapy will be a patient-specific approach. In a recent study, we utilized canine models to demonstrate the feasibility of autologous iNSC generation and implantation on a scale that more closely mirrors human patients (20). The migratory hiNSCs are also genetically engineered to secrete cytotoxic proteins such as tumor necrosis factor-α apoptosis inducing ligand (hiNSC-TRAIL), enabling the cells to track down and kill infiltrating cancer cells after infusion. While one initial study tested the ability of NSCs to reduce peripheral tumor burden in lung cancer (4), the therapeutic potential of hiNSCs for orthotopic breast and lung tumors has not yet been fully explored, despite the prevalence of these diseases. Moreover, no studies have investigated the efficacy of hiNSCs administered intravenously, a much less invasive technique where the ease of infusion and redosing provides significant clinical advantages over intratumoral injections.

Herein we provide the first investigation into the intravenous infusion of rapidly transdifferentiated hiNSCs for the treatment of primary lung and breast cancer. Utilizing kinetic bioluminescence imaging, we show hiNSCs migrate rapidly to both human triple negative breast cancer (TNBC) and non-small cell lung cancer (NSCLC) in co-culture assays. Furthermore, intravenously-infused hiNSCs populated both tumor types in orthotopically-established mouse models of cancer and persisted at the tumor site for 14 days post-infusion. Exploring the anti-tumor efficacy of hiNSC therapy, we show that hiNSC-TRAIL induced dose-dependent killing in co-culture assays. *In vivo*, serial bioluminescence imaging showed that intravenous hiNSC-TRAIL therapy reduced tumor burden while extensive toxicity testing showed the treatment did not induce marked toxicity to healthy tissue. Overall, these results suggest intravenously-infused hiNSC-TRAIL is a safe and effective potential treatment for two of the most common types of cancer.

MATERIALS AND METHODS

Cell lines

NSCLC cell lines A549 and NCI-H460 and hTERT-immortalized human fibroblast line NHF1 were obtained from University of North Carolina Tissue Culture Facility. TNBC cell line MDA-MB-231-Br was obtained via MTA (Toshi Yoneda, PhD). All cell lines were cultured in Dulbecco's modified eagle medium (DMEM; Gibco) supplemented with 10% (v/v) heat inactivated fetal bovine serum (Millipore), 100 Units/mL penicillin (Gibco) and 100 μg/mL streptomycin (Gibco), and 0.01% (v/v) Plasmocin™ (Invivogen). Cell lines were treated for mycoplasma with 0.05% (v/v) Plasmocure™ (Invivogen) for 2 weeks and were tested for mycoplasma with the MycoAlert™ mycoplasma detection kit (Lonza).

hiNSC generation

5×10^4 hTERT-immortalized NHF1s were seeded in 6-well plates and transduced with LV-GFP-TRAIL, LV-GFP-Nano Luciferase (NLuc) (21), or LV-mC-Firefly Luciferase (FLuc) with 8 μg/mL polybrene (Thermo Fisher Scientific) for 12 hours in DMEM supplemented with 10% FBS, 1% penicillin/streptomycin, and 0.01% Plasmocin™. After

initial transduction, cells were transduced with a cocktail of LV-SOX2 and LV-rtTA with polybrene for 12 hours in supplemented DMEM. A week prior to use of cells, 1×10^6 transduced cells were seeded per T175 flask in supplemented DMEM. Cells were cultured in STEMdiff Neural Induction Media (STEMCELL Technologies) with 2 μg/mL doxycycline (Sigma), changing media every other day for 5 days. Cells were detached using Accutase Cell Detachment Solution (STEMCELL Technologies) at room temperature and strained using 100 μm Falcon Cell Strainers (Fisher Scientific). SOX2 expression was verified by staining. Briefly, cells were fixed with 2.5% formalin for 20 minutes and rinsed with PBS. Following incubation in blocking buffer for 1 hour at room temperature, cells were incubated with 1:100 rabbit anti-SOX2 antibody (Abcam) for 1 day at 4°C. After washing thrice with PBS, cells were incubated with 1:1000 goat anti-rabbit cross-adsorbed secondary antibody, Alexa Fluor 568 (Thermo Fisher Scientific) for at least 1 hour. Cells were washed thrice with PBS and incubated in Hoechst for 20 min. Cells were imaged using an EVOS FL Auto Cell Imaging System (Life Technologies).

In vitro therapeutic effects of hiNSC-TRAIL against cancer cell lines

5×10^3 cancer cells (MDA-MB231-Br or A549) labeled with stable expression of FLuc were seeded in 24-well plates in 10% FBS, 1% penicillin/streptomycin, and 0.01% Plasmocin™ DMEM. The following day, wells were seeded with varying numbers of hiNSC-TRAIL cells, from 0 to 10,000 cells/well. After 1, 3, and 7 days, viability of the cancer cells was assessed by adding 0.225 μg/mL XenoLight D-luciferin (PerkinElmer) and measuring luminescence using a SynergyH1 microplate reader (BioTek) at 1-sec per well measurement (N=4) or IVIS® Kinetic (Caliper Life Sciences) (N=4–8). Viability was determined by dividing the luminescent signal of these wells by their untreated counterparts at each time point. To test viability of hiNSCs after exposure to recombinant human TRAIL (Sigma), we incubated hiNSCs expressing FLuc with 1–500 ng/mL TRAIL for 48 hours before assessing luminescence on SynergyH1 microplate reader as described above.

In vitro hiNSC motion and migration

24-well plates were prepared by incubating the empty wells with 10 μg/mL purified mouse laminin (EMD Millipore) in PBS for 12 hours at 37°C. Following incubation, media was aspirated and wells air-dried. Two-chamber cell culture inserts (Ibidi) were placed in each well. 1×10^4 hiNSC-mC-FLuc were seeded on the left side; 2×10^4 A549-GFP-NLuc or MDA-MB231-Br-GFP-NLuc in 80 μL were seeded on the right side of inserts (0.5 mm separation). Control wells (N = 4) had 1×10^4 hiNSC-mC-FLuc were seeded on the left side with nothing in the right insert. Both hiNSCs and tumor cells were cultured in STEMdiff Neural Induction Media (STEMCELL Technologies). 24-hours after seeding cells, inserts were removed, and wells were filled with STEMdiff Neural Induction with 2 μg/mL doxycycline (Sigma) and 2% FBS. Cells were imaged at 10x magnification every 2 hours for 96 hours with EVOS FL Auto Cell Imaging System (Life Technologies). 10 random cells from each beacon were selected and individually tracked over time (ImageJ). Cell tracking data collected in Fiji was uploaded into R for statistical analysis and generation of rose and summary violin plots. Number of cells migrated was determined by manually counting the cells that passed a starting line designated by the leading hiNSC edge at 0 hours.

In vivo bioluminescence imaging

To follow tumor volume or hiNSC-mC-FLuc distribution and persistence, serial bioluminescent imaging (BLI) was performed as previously described (3, 17). Mice were administered D-luciferin (3 mg per mouse in 200 μL of PBS) via intraperitoneal injection. 15 min following injection, photon emission was measured using Ami HT (Spectral Instruments Imaging) or IVIS® Kinetic (Caliper Life Sciences). Luminescence was quantified through analysis with Aura (Spectral Instruments Imaging).

Tissue harvest and processing

Following anesthetization with 5% isoflurane, mice were perfused via intracardiac puncture with 10 mL PBS. Lungs were inflated with 10% neutral buffered formalin (NBF). Lungs, liver, kidneys, and spleen were incubated in 10% NBF for 72 hours before storage in 70% ethanol. Organs were embedded in paraffin, sectioned, and stained with H&E by UNC Animal Histopathology Core and UNC Translational Pathology Laboratory.

In vivo migration studies

For the lung tumor model, A549-GFP-NLuc cells were prepared by washing cells in suspension with PBS and preparing 1.5×10^6 cells in 50 μL 1:1 (v/v) Matrigel matrix (Corning) in PBS. Following anesthetization with isoflurane, female athymic nude mice were placed in a lateral decubitus position. Cells were injected into intercostal space of left lung. Tumor growth was monitored using BLI by intravenous injection of furimazine (Promega; 1:20 v/v in PBS). Tumors grew for two weeks. For the breast tumor model, MDA-MB231-Br-GFP-NLuc were prepared as above and brought to a concentration of 2 million cells in 60 μL 1:1 (v/v) Matrigel matrix (Corning) in PBS. Cells were injected into mammary fat pad. Tumors grew for 10 days. 1×10^6 hiNSC-mC-FLuc cells suspended in 200 μL were intravenously injected. hiNSC-mC-FLuc was followed by BLI following intraperitoneal injection of D-luciferin. hiNSC-mC-FLuc cells were also injected as described above in mice without tumors. Mice were sacrificed at 3, 7, and 14 days after hiNSC-mC-FLuc injection (N=2 per time point). Lungs and fat pad tumors were processed as described above with the following exception: no perfusion was performed prior to removal of lungs to avoid disruption of cells for mice with lung tumors. Lungs and fat pad tumors were incubated in 10% NBF for 24 hours prior to storage in 30% sucrose at 4 °C. Samples were frozen in optimal cutting temperature (OCT) media. Using a cryostat, 10 μm organ sections were collected, stained with Hoechst (Thermo Scientific™), and mounted with ProLong™ Gold Antifade Mountant (Invitrogen). Fluorescent images were collected using Olympus FV3000RS confocal microscope, and fluorescent signal was quantified using ImageJ. All images were optimized for brightness/color contrast.

In vivo therapeutic efficacy studies

Lung H460-mC-FLuc (5×10^4 cells in 30 μL 2:1 Matrigel (v/v) in PBS) or breast MDA-MB231-Br-mC-FLuc were implanted as described above in female athymic nude mice. Tumor volumes were monitored using BLI. Maximum tolerated dose of 1×10^6 hiNSC-TRAIL cells suspended in 200 μL PBS were injected intravenously 4 and 8 days after H460 tumor implantation or 5 days after MDA-MB231-Br implantation. The orthotopic H460

tumor study was completed twice to increase N, and multiple unpaired t-tests were used to determine no significant difference between controls and hiNSC-TRAIL groups of the first and second studies. Mice without visible thoracic tumors with a 2-second exposure via BLI by Day 14 were excluded. BLI values for individual days were excluded if a value dropped by an order of magnitude from previous time point and then increased by about an order of magnitude by the next time point, presumably because of a poor intraperitoneal injection of luciferin. N = 15 was used for controls, and N = 16 was used for treatment mice with H460 tumors. N = 5 for treated mice and N = 4 for control mice with MDA-MB231-Br tumors. Grubbs' test was used to identify outliers, and these mice were excluded. Mice were sacrificed when they lost >20% of their highest body weight, exhibited signs of distress, or if a visible tumor exceeded 2 cm in length. Survival is reported as median with 95% confidence intervals (CI) of median. Survival data reported for the H460 model are from the second study. The study was ended after 100 days for the MDA-MB231-Br model.

In vivo toxicity studies

To test the toxicity of either carrier hiNSC-mC-FLuc or cytotoxic hiNSC-TRAIL, 1×10^6 hiNSC-mC-FLuc or 1×10^6 hiNSC-TRAIL cells in 200 μL PBS were injected intravenously into female athymic nude mice (N = 4 per time point). 3, 7, 14, and 28 days following injection, 700 μL of blood was collected via intercostal puncture, and organs were harvested following perfusion with PBS. Blood was collected in K_2 EDTA Microtainer™ (BD) and in clot activator Microtainer™ (BD), from which serum was extracted. Blood and serum samples were analyzed by the UNC Animal Histopathology Core.

Ethics statement

All experimental mouse protocols were previously approved by the Institutional Animal Care and Use Committees at University of North Carolina -- Chapel Hill.

Statistics

Data were analyzed using GraphPad Prism and R. Multiple unpaired t-tests without correction for multiple comparisons were used to compare two groups. Multiple groups were analyzed by one-way ANOVA, followed by Dunnett's post-hoc test. Survival analysis was conducted using a Log-rank test. Unless otherwise specified, all values are expressed as mean +/− SEM, and differences were considered significant when $P < 0.05$.

RESULTS

Assessing hiNSC migration towards lung cancer and breast cancer *in vitro*

One of the most unique and beneficial attributes of hiNSC therapy is the ability of the cells to actively seek out and populate local and distant tumors. This ability has been proven extensively in mouse models of brain cancer where hiNSC are directly infused into brain tissue (17). However, it is unknown whether SOX2-expressing hiNSCs (Supplementary Figure 1) exhibit similar homing capability to extracranial tumors or whether their tumor-homing capacity remains intact when infused intravenously into the blood stream. To answer these questions, we first investigated the tumoritropic properties of hiNSCs to TNBC and NSCLC cells using our mixed culture models where hiNSC migration is tracked in

real-time. hiNSC-mC-FLuc cells were seeded 500 μm apart from A549-GFP-FLuc lung human cancer cells or MDA-MB231-Br-GFP-FLuc human TNBC cells in two-chamber cell culture inserts (Figure 1A). 24 hrs after seeding, the culture inserts were removed and kinetic high-resolution images were captured every 2 hours for 96 hrs to track the movement of hiNSC towards the cancer cells. Analysis of time-lapse images show that hiNSCs directionally migrated towards both A549 and MDA-MB231-Br cells (Figure 1B). Quantification further supported kinetic imaging results, showing a mean of 14 and 29 cells migrated past a starting line designated by the leading edge of the hiNSCs at time 0 towards A549 and MDA-MB231-Br, respectively, at 96 hrs compared to an average of only 3 cells in control wells where hiNSCs were plated without nearby tumor cells (Figure 1C). Single cell migratory path analysis of directionality showed the mean directionality index was 0.300 ± 0.016 and 0.352 ± 0.022 for migrating hiNSCs towards A549 and MDA-MB231-Br compared to 0.166 ± 0.017 in control wells. The hiNSCs seeded adjacent to either A549 or MDA-MB231-Br showed farther mean final cell displacement (180 ± 11 or 205 ± 14 μm, respectively) than hiNSCs seeded without nearby tumor cells (112 ± 13 μm) (Figure 1D–F). Directional migration of hiNSCs was also observed toward H460 NSCLC cells (Supplementary Figure 2A–C) while non-transdifferentiated fibroblasts did not show enhanced tropism toward H460 cells over the control (Supplementary Figure 3A–B). In addition, we did not observe significant directional movement of hiNSCs toward non-tumor cell lines (Supplementary Figure 4). These data suggest hiNSCs possess tumor homing capability toward TNBC and NSCLC cell lines *in vitro*.

Investigating hiNSC migration towards NSCLC and TNBC tumors *in vivo*

In human patients, the majority of cell therapies are infused intravenously for the treatment of peripheral tumor types (22). As we found hiNSCs migrate to both TNBC and NSCLC in co-cultures, we sought to explore the ability of hiNSCs to target both tumor types *in vivo* following intravenous infusion and determine the residence time of the cells at the tumor. We first established either A549-GFP-NLuc orthotopic lung tumors or MDA-MB231-Br-GFP-NLuc fat pad tumors in athymic nude mice (Figure 2A–B). Once tumor establishment was confirmed by serial imaging, 1×10^6 hiNSC-mC-FLuc cells were administered intravenously into tumor-bearing mice, and hiNSC distribution was monitored by firefly luciferase BLI. In animals with orthotopic lung cancer xenografts, analysis of BLI signal showed hiNSCs were detectable at tumor foci in the thorax shortly after infusion. Thoracic BLI signal gradually declined over 11 days in mice both with and without tumors (Figure 2C, Supplementary Figure 5). To visualize hiNSCs at levels below the limit of detection by BLI, we performed fluorescent microscopic analysis of tissue sections from a subset of mice sacrificed at each time point. Our high-resolution imaging showed hiNSC-mC-FLuc were present and co-localized with NSCLC GFP+ tumor within 3 days post-injection and could still be detected 14 days post-infusion (Figure 2C, E). In mice bearing TNBC tumors, fluorescent analysis showed hiNSCs were detected at the tumor by day 3, reached peak accumulation at day 7, and gradually declined through day 14 (Figure 2D, F). Fluorescent analysis was used to characterize migration of hiNSCs toward TNBC tumors because the BLI signal of these cells was below the limit of detection. In both tumor models, hiNSCs were observed to colocalize to tumors within 3 days and persisted for at least 14 days.

Exploring the efficacy of intravenous hiNSC therapy for lung and breast cancer *in vitro*

To take advantage of the hiNSCs' tumor-homing migratory capabilities, we produced a line of hiNSC-TRAIL to test the ability of hiNSCs to deliver therapeutics to tumors. We performed co-culture assays with ratios ranging from 10:1 to 1:5 of tumor cells (NSCLC H460 or TNBC MDA-MB231-Br) to hiNSC-TRAIL cells for up to 7 days (Figure 3A). Cell viability assays and summary graphs showed hiNSC-TRAIL cells significantly reduced both H460 and MDA-MB231-Br tumor cells in a dose- and time-dependent manner. Viability as a percentage of control is presented in Figure 3B–C, and raw luminescent values are presented in Supplementary Figure 6A–B. To next investigate the kinetics of the tumor-killing by hiNSC-TRAIL, we performed real-time serial imaging of tumor cell viability when incubated with hiNSC-TRAIL cells (Figure 3D–G). Analysis of kinetic killing curves showed a left-shift in the curve with increasing concentrations of hiNSC-TRAIL cells for both tumor cell lines, indicating tumor killing in a rapid and dose-dependent manner. At a 1:1 ratio of tumor: hiNSC-TRAIL, we found the therapy required 42 and 18 hours to induce 50% reduction in tumor cell signal of H460 and MDA-MB231-Br, respectively. Despite initial differences in the rate of tumor kill, fluorescent images captured 96 hrs post-treatment showed hiNSC-TRAIL therapy was able to reduce tumor cell signal by >98% relative to non-treated cells at the highest dose. Taken together, these data suggest hiNSC-TRAIL therapy induces killing of both TNBC and NSCLC cells. Importantly, decreasing the tumor: hiNSC-TRAIL ratio not only increased the percentage of tumor cells killed, but also the rate at which the tumor cells died.

Investigating hiNSC therapy for NSCLC and TNBC *in vivo*

To investigate the efficacy of intravenous hiNSC therapy for lung and breast cancer, we tested the efficacy of hiNSC-TRAIL therapy against primary NSCLC and TNBC *in vivo*. Orthotopic H460-mC-FLuc or MDA-MB231-Br-mC-FLuc tumors were established in the lungs or fat pad of nude mice, respectively. One week after tumor implant, 1×10^6 hiNSC-TRAIL cells or control hiNSC-GFP cells were injected intravenously (Figure 4A–B). In mice bearing orthotopic H460 tumors established in the lungs, mice treated with hiNSC-TRAIL showed a significant reduction in tumor volume days 7 and 14 after the first dose of intravenous hiNSCs; the mean tumor volumes of mice treated with hiNSC-TRAIL were 33.1% and 29.8% of the volumes of control-treated animals 7 and 14 days post-treatment, respectively (Figure 4C, E, Supplementary Figure 7A). The highly aggressive nature of this model led to rapid tumor rebound, though we did observe a modest trend toward improvement in overall median survival (49 days with 95% CI 24 – 104 days for mice treated with hiNSC-TRAIL; 35.5 days with 95% CI 22 – 82 days for control mice) (Figure 4G). hiNSC-TRAIL therapy induced strong tumor kill in TNBC tumors. Serial imaging showed mice with human TNBC infused with hiNSC-TRAIL therapy had a mean tumor volume of 28.2% and 7.3% compared to control-treated animals 21 days and 36 days post-treatment, respectively (Figure 4D, F, Supplementary Figure 7B–D). For both tumor models, we observed significant reductions in tumor volumes in mice treated with intravenous hiNSC-TRAIL based on multiple unpaired t-tests without correction for multiple comparisons. Given the large number of time points, when a two-stage setup was used to correct for multiple comparisons, the adjusted p-values were >0.05. A strong though non-significant trend toward increased median survival was observed (100 days with 95% CI

64 – 100 days for TNBC mice treated with hiNSC-TRAIL; 44 days with 95% CI 44 – 100 days for control mice) (Figure 4H).

hiNSC and TRAIL toxicity

In order to determine the safety of hiNSC therapy, we had previously characterized both immortalized fibroblasts (17) and non-immortalized patient fibroblasts (19), in which we observed no oncolytic transformation. To further investigate the safety of hiNSC therapy, we infused a single maximum tolerated dose of either non-therapeutic hiNSC-mC-FLuc or therapeutic hiNSC-TRAIL to evaluate the impact of both the cell carriers and the carrier + drug, respectively. On subsequent days over a 28-day time-course post-infusion, lung, kidney, liver, and spleen were harvested, and histology, hematology, and blood chemistry values were evaluated and compared to blank, non-infused mice. H&E histochemistry of major organs demonstrated all examined organs were within normal limits regardless of whether the mice received the carrier + drug or the carrier alone. Rare, scattered cell clusters with large nuclei were identified within alveolar septal walls of lungs harvested from early time points in the post-infusion and carrier + drug groups; these are presumed to be the infused hiNSCs. The cell clusters were no longer observed in either Day 28 sample. Non-specific lymphocytic infiltration in liver samples was moderately increased in hiNSC-infused mice compared to blank, non-infused mice. Spleen samples in both groups showed moderately increased follicle size with occasional formation of germinal centers at each time point with the most activity seen in mice 3 days after infusion with the carrier. We speculate that hepatic lymphocytic and splenic responses are likely due to murine immune responses against human hiNSC infusion. Minimal interstitial nephritis was occasionally observed in the kidneys of mice infused with the carrier (Figure 5). Hematology and blood chemistry values showed no significant sustained alterations in hiNSC-infused mice compared to blank mice (Table 1). Mice infused with carrier only showed mild, transient increases in creatinine that resolved within 28 days of infusion. Minor transient decreases in BUN and creatinine were observed in mice infused with carrier + drug that each resolved. Taken together, the pathology, hematology, and clinical chemistry values indicate no significant toxic effects of either carrier or carrier + drug following intravenous infusion. TRAIL itself is only toxic to hiNSCs or fibroblasts at concentrations (Supplementary Figure 8A–B) well above documented levels achieved through production by hiNSCs, about 2 fg TRAIL/cell/hr (19) except if hiNSC-TRAIL outnumbers tumor cells 50:1 (Supplementary Figure 8C). TUNEL stains indicated no significant apoptosis in healthy tissue following intravenous infusion of hiNSC-TRAIL (Supplementary Figure 9A–D).

DISCUSSION

In this study, we investigated the ability of human fibroblasts that were rapidly transdifferentiated into hiNSCs to home to and kill primary NSCLC or TNBC tumors following intravenous infusion. While previous studies have investigated the use of hiNSCs to treat glioblastoma (17, 18) or other types of stem cells to treat extracranial tumors (4, 23–25), to our knowledge, this study marks the first effort to treat primary breast or lung tumors with hiNSCs. Migration of hiNSCs has been well-characterized in the brain parenchyma (18, 26), but this is the first study to investigate the distribution of

intravenously-administered hiNSCs. Our *in vitro* results show directional migration of hiNSCs toward both TNBC and NSCLC. Given that minimal and non-directional migration was observed in the control group, we infer the migration observed toward the cancer lines was not merely random motion or cell proliferation. hiNSCs are thought to follow chemokine gradients produced by tumor cells or surrounding areas of hypoxia (6), and we expected that an increasing number of hiNSCs would migrate toward cancer cells as the chemokine gradient is produced over time. While the number of migrating cells toward NSCLC was not significantly different between the control and treatment groups, the number of migrating hiNSCs toward tumor cells trended toward an increase over time to tumors, and significantly more hiNSCs migrated toward TNBC cells than controls. However, counting cells that pass the starting line discounts movement of cells that start far from the starting line. To account for differences in starting position, we also report directionality and displacement. We observed significantly increased directionality indices and final displacements of hiNSCs toward both tumor lines than in the control group, suggesting hiNSCs do migrate to both NSCLC and TNBC *in vitro*. To determine if these *in vitro* results translate to an *in vivo* setting, we tested the migration of hiNSCs to TNBC fat pad tumors or NSCLC lung tumors. We observed co-localization of hiNSCs at both NSCLC and TNBC tumor foci as early as 3 days and as late as 14 days after intravenous infusion. This suggests the cells not only migrate to tumors quickly but also persist, albeit at low levels, for a relatively long period of time. These persistence results are consistent with our previous studies of hiNSCs in the brains of mice (17), and an autologous infusion of iNSCs likely would increase persistence even more, as our previous canine iNSC study showed persistence for more than 80 days (20). The presence of a tumor does not appear to significantly impact hiNSC persistence or overall distribution, consistent with similar studies with MSCs (27). Importantly, our results here also suggest the migratory ability of hiNSCs is not limited by a specific tumor line as we observed migration toward both NSCLC and TNBC cells. These results indicate the versatility of these therapeutic hiNSCs to target a variety of primary tumors extracranially.

Our *in vitro* co-culture killing assay demonstrated that both NSCLC and TNBC cell lines are sensitive to cytotoxic TRAIL. TRAIL has been shown to increase the activity of caspase 3 and 9 as well as annexin V and PI in tumor lines such as the NSCLC line H460 (28). However, the TNBC line was much more sensitive to TRAIL than the NSCLC line. Differential TRAIL resistance for various tumor lines has been widely documented (29–33), and so partial resistance to TRAIL is not unexpected. Thus, in the proceeding experiments, we anticipated that the TNBC line would respond better to hiNSC-TRAIL than the NSCLC line. Despite the partial sensitivity to TRAIL observed in our *in vitro* studies and the highly invasive nature of the NSCLC line, the NSCLC tumors *in vivo* did respond well to hiNSC-TRAIL therapy. Both the mice with TNBC tumors and those with NSCLC that were treated with hiNSC-TRAIL therapy did show a reduction in the tumor BLI signal within 2 weeks of the initial infusion. Mice with NSCLC tumors treated with hiNSC-TRAIL therapy trended toward increased survival, likely limited by the tumor line's partial TRAIL resistance. We also saw a strong trend toward increased survival of mice with TNBC tumors treated with hiNSC-TRAIL, indicating the potential of this therapy in a TRAIL-sensitive tumor model.

While TRAIL is a useful cytotoxic protein for proof-of-concept studies and is well-tolerated in humans (34), hiNSCs are not limited to using a monotherapy with TRAIL. Given the prevalence of tumor resistance to TRAIL (25, 30, 31, 33, 35–37), potential next steps include combining TRAIL with a drug/prodrug system. Our lab has previously shown that hiNSCs can be engineered to produce the prodrug-activator thymidine kinase, which has shown good results against glioblastoma *in vivo* (3, 17). In this treatment paradigm, if a tumor shows resistance to TRAIL, a prodrug can be administered to initiate an additional therapy. Another option is to combine hiNSC-TRAILs with radiation therapy. Given the prevalence of radiation therapy to treat both NSCLC and TNBC (38–41), it will be key to study this interaction in the future. In this treatment paradigm, hiNSC-TRAIL would scavenge remaining tumor sites post-radiation. Furthermore, radiation can sensitize tumors to TRAIL (33) and promote migration by increasing expression of hypoxic and inflammatory markers (6, 42–44).

The therapeutic effect of hiNSC-TRAIL cells was limited in this model by the flow of cells through vessels. Our results indicate that intravenously-infused hiNSCs immediately travel to the lungs and persist for at least two weeks. Our cell therapy takes advantage of this first pass through the lungs in the case of treating orthotopic lung tumors. We anticipate we would observe a stronger therapeutic effect in the case of TNBC if the cells were able to pass through the lungs more quickly. Previous studies have indicated that smaller cells, such as bone marrow-derived mononuclear cells (BMMC) with a cell volume of 150 μm^3, are more likely to pass through the lungs into arterial circulation than larger cells, such as NSCs with a cell volume of about 2500 μm^3 (45). Human T-cells, which have a volume the same order of magnitude as BMMCs (46), have been shown to distribute throughout the mouse following intravenous infusion in a similar fashion to a human (47). Thus, we anticipate the reason for the persistence of our human hiNSCs in the lungs of mice is due at least in part to the large hiNSCs being unable to pass through small mouse lung capillaries (48, 49).

Despite the lengthy persistence of hiNSCs in the lungs, they do not appear to cause significant toxicity. Following infusion of hiNSCs, there was no concerning inflammatory response observed in the lungs, liver, kidneys, or spleen. Only mild reactive changes were observed in the germinal centers of the spleen at early post-infusion time points that appear to decrease over time. Elevated creatinine levels returned to baseline 1 month after infusion. This correlates with our previous canine study in which induced neural stem cells transdifferentiated from canine fibroblasts showed no signs of significant iNSC-related tissue abnormality for greater than 84 days after injection (20). When compared to the significant toxicities associated with current chemotherapies such as taxol (50), the variations we observed from baseline in histology, hematology, and clinical chemistry values after infusion are comparably mild and transient.

While we recognize the limitations of our current model, we still observed migration to both NSCLC and TNBC tumors following intravenous infusion of hiNSCs. To our knowledge, this is the first study to investigate the potential of any NSC to treat NSCLC following intravenous infusion. Furthermore, this is the first study to use hiNSCs to treat either NSCLC or TNBC. Mice with TNBC or NSCLC tumors showed significant reduction following intravenous hiNSC-TRAIL therapy. To further improve the therapeutic efficacy

of these cells, we are currently in the process of developing a second generation of hiNSCs with more rapidly migrating cells and increased residence time. Moreover, future studies should also examine the impact of hiNSCs on patient-derived tumors. Overall, these are promising findings in the development of this cell therapy with implications to treat a variety of different cancers.

Supplementary Material

Refer to Web version on PubMed Central for supplementary material.

ACKNOWLEDGMENTS

The authors would like to thank the Biomedical Research Imaging Center, the Tissue Pathology Laboratory, the Animal Histopathology Core, the Histology Research Core, and the Neuroscience Microscopy Core at The University of North Carolina-Chapel Hill. Schematic figures were made using BioRender. The authors would also like to thank Dr. Chad Pecot's lab and Michael Marand. This work was supported by Eshelman Institute for Innovation and the National Cancer Institute of the National Institutes of Health under Award Number F30CA243270. The content is solely the responsibility of the authors and does not necessarily represent the official views of the National Institutes of Health.

COI:

K.T.S. and S.D.H have an ownership interest in Falcon Therapeutics, Inc., which has licensed aspects of hiNSC technology from the University of North Carolina at Chapel Hill. C.K.A. has research funding from PUMA, Lilly, Merck, Seattle Genetics, Nektar, Tesaro, and G1-Therapeutics. C.K.A. has compensated consulting roles from Genentech, Eisai, IPSEN, and Seattle Genetics with royalties from UpToDate, and Jones and Bartlett. A.R.M.S., W.J., J.R.B., A.V., S.A.M., M.T., and A.S.W., have no conflicts to disclose.

REFERENCES

1. Siegel RL, Miller KD, Jemal A, Cancer statistics, 2018, CA. Cancer J. Clin 68, 7–30 (2018).
2. Aboody KS, Brown a, Rainov NG, Bower K. a, Liu S, Yang W, Small JE, Herrlinger U, Ourednik V, Black PM, Breakefield XO, Snyder EY, Neural stem cells display extensive tropism for pathology in adult brain: evidence from intracranial gliomas., Proc. Natl. Acad. Sci. U. S. A 97, 12846–12851 (2000). [PubMed: 11070094]
3. Bagó JR, Sheets KT, Hingtgen SD, Neural stem cell therapy for cancer, Methods 99, 37–43 (2016). [PubMed: 26314280]
4. Yi B-R, Kim SU, Choi K-C, Co-treatment with therapeutic neural stem cells expressing carboxyl esterase and CPT-11 inhibit growth of primary and metastatic lung cancers in mice, Oncotarget 5, 12835–12848 (2014). [PubMed: 25544747]
5. Hong SH, Lee HJ, An J, Lim I, Borlongan C, Aboody KS, Kim SU, Human neural stem cells expressing carboxyl esterase target and inhibit tumor growth of lung cancer brain metastases, Cancer Gene Ther 20, 678–682 (2013). [PubMed: 24310061]
6. Zhao D, Najbauer J, Garcia E, Metz MZ, Gutova M, Glackin CA, Kim SU, Aboody KS, Neural Stem Cell Tropism to Glioma: Critical Role of Tumor Hypoxia, Mol. Cancer Res 6, 1819–1829 (2008). [PubMed: 19074827]
7. Kim SK, Kim SU, Park IH, Bang JH, Aboody KS, Wang KC, Cho BK, Kim M, Menon LG, Black PM, Carroll RS, Human neural stem cells target experimental intracranial medulloblastoma and deliver a therapeutic gene leading to tumor regression, Clin. Cancer Res 12, 5550–5556 (2006). [PubMed: 17000692]
8. Aboody KS, Najbauer J, Metz MZ, D'Apuzzo M, Gutova M, Annala AJ, Synold TW, Couture LA, Blanchard S, Moats RA, Garcia E, Aramburo S, V Valenzuela V, Frank RT, Barish ME, Brown CE, Kim SU, Badie B, Portnow J, Neural stem cell-mediated enzyme/prodrug therapy for glioma: preclinical studies., Sci. Transl. Med 5, 184ra59 (2013).

9. Portnow J, Synold TW, Badie B, Tirughana R, Lacey SF, D'apuzzo M, Metz MZ, Najbauer J, Bedell V, Vo T, Gutova M, Frankel P, Chen M, Aboody KS, Neural stem cell-based anti-cancer gene therapy: a first-in-human study in recurrent high grade glioma patients, Clin. Cancer Res (2016), doi:10.1158/1078-0432.CCR-16-1518.
10. Gutova M, Flores L, Adhikarla V, Tsaturyan L, Tirughana R, Aramburo S, Metz M, Gonzaga J, Annala A, Synold TW, Portnow J, Rockne RC, Aboody KS, Quantitative Evaluation of Intraventricular Delivery of Therapeutic Neural Stem Cells to Orthotopic Glioma, Front. Oncol 9, 1–8 (2019). [PubMed: 30761267]
11. Metz MZ, Gutova M, Lacey SF, Abramyants Y, Vo T, Gilchrist M, Tirughana R, Ghoda LY, Barish ME, Brown CE, Najbauer J, Potter PM, Portnow J, Synold TW, Aboody KS, Neural Stem Cell-Mediated Delivery of Irinotecan-Activating Carboxylesterases to Glioma: Implications for Clinical Use MARIANNE, Stem Cells Transl. Med 2, 983–992 (2013). [PubMed: 24167321]
12. van Eekelen M, Sasportas LS, Kasmieh R, Yip S, Figueiredo J-L, Louis DN, Weissleder R, Shah K, Human stem cells expressing novel TSP-1 variant have anti-angiogenic effect on brain tumors., Oncogene 29, 3185–95 (2010). [PubMed: 20305695]
13. Kim SK, Cargioli TG, Machluf M, Yang W, Sun Y, Al-Hashem R, Kim SU, Black PM, Carroll RS, PEX-producing human neural stem cells inhibit tumor growth in a mouse glioma model, Clin. Cancer Res 11, 5965–5970 (2005). [PubMed: 16115940]
14. Cheng Y, Morshed R, Cheng S-H, Tobias A, Auffinger B, Wainwright DA, Zhang L, Yunis C, Han Y, Chen C-T, Lo L-W, Aboody KS, Ahmed AU, Lesniak MS, Nanoparticle-programmed self-destructive neural stem cells for glioblastoma targeting and therapy., Small 9, 4123–9 (2013). [PubMed: 23873826]
15. Rainov NG, A Phase III Clinical Evaluation of Herpes Simplex Virus Type 1 Thymidine Kinase and Ganciclovir Gene Therapy as an Adjuvant to Surgical Resection and Radiation in Adults with Previously Untreated Glioblastoma Multiforme, Hum. Gene Ther 11, 2389–2401 (2002).
16. Morizane A, Doi D, Kikuchi T, Okita K, Hotta A, Kawasaki T, Hayashi T, Onoe H, Shiina T, Yamanaka S, Takahashi J, Direct Comparison of Autologous and Allogeneic Transplantation of iPSC-Derived Neural Cells in the Brain of a Nonhuman Primate, Stem Cell Reports 1, 283–292 (2013). [PubMed: 24319664]
17. Bago J, Okolie O, Dumitru R, Ewend MG, Parker JS, Vander Werff R, Underhill TM, Schmid RS, Miller CR, Hingtgen SD, Tumor-homing cytotoxic human induced neural stem cells for cancer therapy, Sci. Transl. Med 6510, 1–14 (2017).
18. Bagó JR, Alfonso-Pecchio A, Okolie O, Dumitru R, Rinkenbaugh A, Baldwin AS, Miller CR, Magness ST, Hingtgen SD, Therapeutically engineered induced neural stem cells are tumour-homing and inhibit progression of glioblastoma, Nat. Commun 7 (2016), doi:10.1038/ncomms10593.
19. Buckley A, Hagler SB, Lettry V, Bagó JR, Maingi SM, Khagi S, Ewend MG, Miller CR, Hingtgen SD, Generation and Profiling of Tumor-Homing Induced Neural Stem Cells from the Skin of Cancer Patients, Mol. Ther 28, 1614–1627 (2020). [PubMed: 32402245]
20. Bomba HN, Sheets KT, Valdivia A, Khagi S, Ruterbories L, Mariani CL, Borst LB, Tokarz DA, Hingtgen SD, Personalized-induced neural stem cell therapy: Generation, transplant, and safety in a large animal model, Bioeng. Transl. Med, 1–16 (2020).
21. Schaub FX, Reza MS, Flaveny CA, Li W, Musicant AM, Hoxha S, Guo M, Cleveland JL, Amelio AL, Fluorophore-NanoLuc BRET reporters enable sensitive In Vivo optical imaging and flow cytometry for monitoring tumorigenesis, Cancer Res 75, 5023–5033 (2015). [PubMed: 26424696]
22. Approved Cellular and Gene Therapy ProductsU.S. Food Drug Adm (2019) (available at https://www.fda.gov/vaccines-blood-biologics/cellular-gene-therapy-products/approved-cellular-and-gene-therapy-products).
23. Zhao D, Najbauer J, Annala AJ, Garcia E, Metz MZ, Gutova M, Polewski MD, Gilchrist M, Glackin CA, Kim SU, Aboody KS, Human neural stem cell tropism to metastatic breast cancer, Stem Cells 30, 314–325 (2012). [PubMed: 22084033]
24. Mooney R, Hammad M, Batalla-Covello J, Abdul Majid A, Aboody KS, Stem Cells Translational Medicine Concise Review: Neural Stem Cell-Mediated Targeted Cancer Therapies, Stem Cells Transl. Med, 740–747 (2018). [PubMed: 30133188]

25. Lee JC, Lee WH, Min YJ, Cha HJ, Han MW, Chang HW, Kim SA, Choi SH, Kim SW, Kim SY, Development of TRAIL resistance by radiation-induced hypermethylation of DR4 CpG Island in recurrent laryngeal squamous cell carcinoma, Int. J. Radiat. Oncol. Biol. Phys 88, 1203–1211 (2014). [PubMed: 24661673]
26. Okolie O, Irvin DM, Bago JR, Sheets K, Satterlee A, Carey-Ewend AG, Lettry V, Dumitru R, Elton S, Ewend MG, Ryan Miller C, Hingtgen SD, Intra-cavity stem cell therapy inhibits tumor progression in a novel murine model of medulloblastoma surgical resection, PLoS One 13, 1–16 (2018).
27. Albarenque SM, Zwacka RM, Mohr A, Both human and mouse mesenchymal stem cells promote breast cancer metastasis, Stem Cell Res 7, 163–171 (2011). [PubMed: 21763624]
28. Xia P, Wang W, Bai Y, Claudin-7 suppresses the cytotoxicity of TRAIL-expressing mesenchymal stem cells in H460 human non-small cell lung cancer cells, Apoptosis 19, 491–505 (2014). [PubMed: 24242915]
29. Zhang L, Fang B, Mechanisms of resistance to TRAIL-induced apoptosis in cancer, Cancer Gene Ther 12, 228–237 (2005). [PubMed: 15550937]
30. Trivedi R, Mishra DP, Trailing TRAIL Resistance: Novel Targets for TRAIL Sensitization in Cancer Cells, Front. Oncol 5 (2015), doi:10.3389/fonc.2015.00069.
31. Wang F, Lin J, Xu R, The Molecular Mechanisms of TRAIL Resistance in Cancer Cells: Help in Designing New Drugs, Curr. Pharm. Des 20, 6714–6722 (2014). [PubMed: 25269558]
32. Stegehuis JH, de Wilt LHAM, de Vries EGE, Groen HJ, de Jong S, Kruyt FAE, TRAIL receptor targeting therapies for non-small cell lung cancer: current status and perspectives., Drug Resist. Updat 13, 2–15 (2010). [PubMed: 20036602]
33. Marini P, Schmid A, Jendrossek V, Faltin H, Daniel PT, Budach W, Belka C, Irradiation specifically sensitises solid tumour cell lines to TRAIL mediated apoptosis, BMC Cancer 5, 1–11 (2005). [PubMed: 15631637]
34. Herbst RS, Eckhardt SG, Kurzrock R, Ebbinghaus S, O'Dwyer PJ, Gordon MS, Novotny W, Goldwasser MA, Tohnya TM, Lum BL, Ashkenazi A, Jubb AM, Mendelson DS, Phase I dose-escalation study of recombinant human Apo2L/TRAIL, a dual proapoptotic receptor agonist, in patients with advanced cancer, J. Clin. Oncol 28, 2839–2846 (2010). [PubMed: 20458040]
35. Dimberg LY, Anderson CK, Camidge R, Behbakht K, Ford HL, counteracting resistance against TRAIL-based therapeutics, 32, 1341–1350 (2015).
36. Nesterenko I, Wanningen S, Bagci-Onder T, Anderegg M, Shah K, Evaluating the Effect of Therapeutic Stem Cells on TRAIL Resistant and Sensitive Medulloblastomas, PLoS One 7, 1–9 (2012).
37. Huang Y, Yang X, Xu T, Kong Q, Zhang Y, Shen Y, Wei Y, Wang G, Chang KJ, Overcoming resistance to TRAIL-induced apoptosis in solid tumor cells by simultaneously targeting death receptors, c-FLIP and IAPs, Int. J. Oncol 49, 153–163 (2016). [PubMed: 27210546]
38. Steward LT, Gao F, Taylor MA, Margenthaler JA, Impact of radiation therapy on survival in patients with triple-negative breast cancer, Oncol. Lett 7, 548–552 (2014). [PubMed: 24396485]
39. Lu JY, Lin PX, Huang BT, Calculating the individualized fraction regime in stereotactic body radiotherapy for non-small cell lung cancer based on uncomplicated tumor control probability function, Radiat. Oncol 14, 1–9 (2019). [PubMed: 30621744]
40. Yao Y, Chu Y, Xu B, Hu Q, Song Q, Radiotherapy after surgery has significant survival benefits for patients with triple-negative breast cancer, Cancer Med 8, 554–563 (2019). [PubMed: 30632300]
41. Cheng M, Jolly S, Quarshie WO, Kapadia N, Vigneau FD, Kong FM, Modern radiation further improves survival in non-small cell lung cancer: An analysis of 288,670 patients, J. Cancer 10, 168–177 (2019). [PubMed: 30662537]
42. Kim SM, Oh JH, Park SA, Rhu CH, Lim JY, Kim DS, Chang JW, Oh W, Jeun SS, Irradiation enhances the tumor tropism and therapeutic potential of tumor necrosis factor-related apoptosis-inducing ligand-secreting human umbilical cord blood-derived mesenchymal stem cells in glioma therapy, Stem Cells 28, 2217–2228 (2010). [PubMed: 20945331]
43. Friedman E, Immune Modulation by Ionizing Radiation and its Implications for Cancer Immunotherapy, Curr. Pharm. Des 8, 1765–1780 (2005).

44. Thomas JG, Kerrigan BCP, Hossain A, Gumin J, Shinojima N, Nwajei F, Ezhilarasan R, Love P, Sulman E, Lang FF, Ionizing radiation augments glioma tropism of mesenchymal stem cells, J. Neurosurg 128, 287–295 (2018). [PubMed: 28362237]

45. Fischer UM, Harting MT, Jimenez F, Monzon-Posadas WO, Xue H, Savitz SI, Laine GA, Cox CS, Pulmonary Passage is a Major Obstacle for Intravenous Stem Cell Delivery: The Pulmonary First-Pass Effect, Stem Cells Dev 18, 683–692 (2008).

46. Chapman EH, Kurec AS, Davey FR, Cell volumes of normal and malignant mononuclear cells, J. Clin. Pathol 34, 1083–1090 (1981). [PubMed: 6975780]

47. Parente-Pereira AC, Burnet J, Ellison D, Foster J, Davies DM, Van Der Stegen S, Burbridge S, Chiapero-Stanke L, Wilkie S, Mather S, Maher J, Trafficking of CAR-Engineered human T cells following regional or systemic adoptive transfer in SCID beige mice, J. Clin. Immunol 31, 710–718 (2011). [PubMed: 21505816]

48. Knust J, Ochs M, Gundersen HJG, Nyengaard JR, Stereological estimates of alveolar number and size and capillary length and surface area in mice lungs, Anat. Rec 292, 113–122 (2009).

49. Levitzky MG, in Pulmonary Physiology, 8e, (The McGraw-Hill Companies, New York, NY, 2013).

50. Marupudi NI, Han JE, Li KW, Renard VM, Tyler BM, Brem H, Paclitaxel: A review of adverse toxicities and nov el delivery strategies, Expert Opin. Drug Saf 6, 609–621 (2007) [PubMed: 17877447]

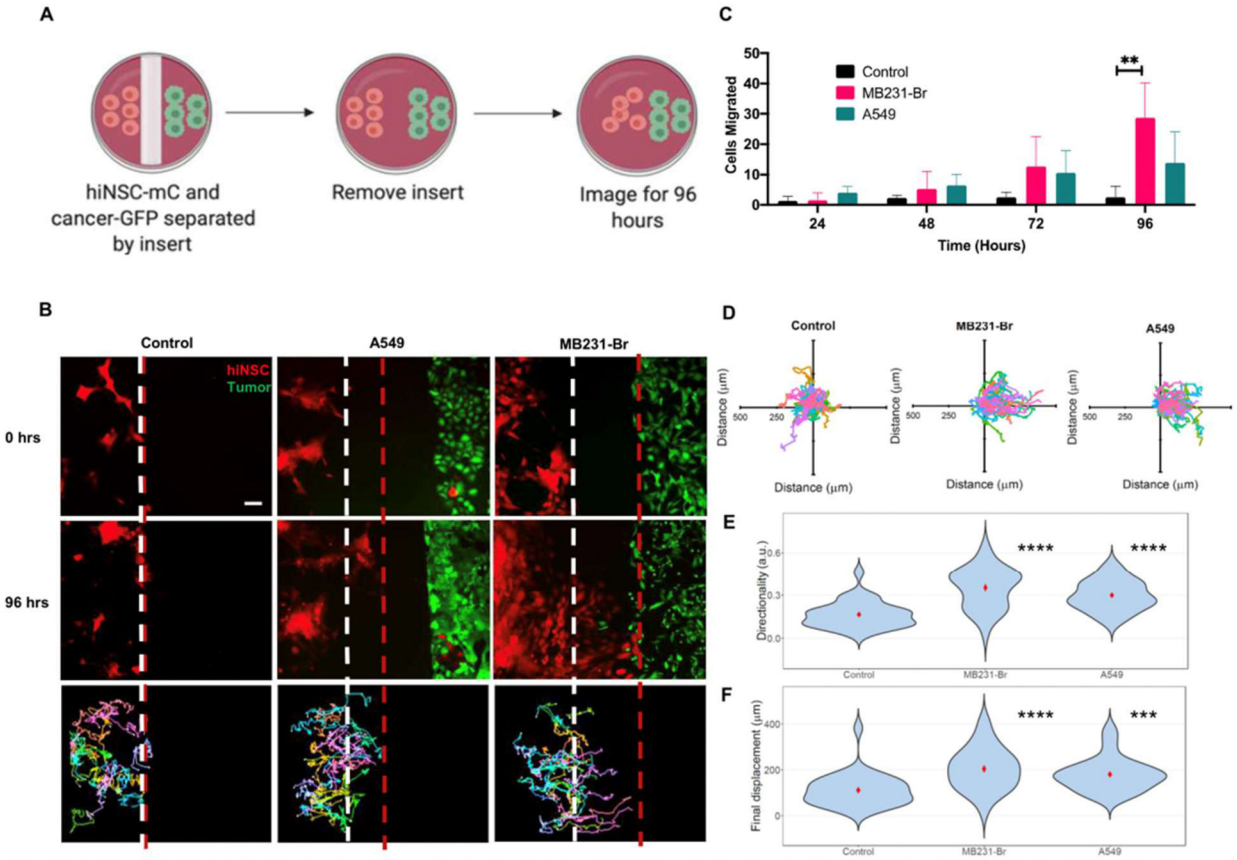

Figure 1.

In vitro migration of hiNSC toward tumor cells. (A) Schematic of two-chamber wells to observe migration of hiNSCs (left) and tumor cells (right). (B) Fluorescent image of movement of hiNSCs (red) after 0 and 96 hours, adjacent to tumors cells A549 or MDA-MB231-Br (green) or nothing (control). The white dotted line indicates the position of hiNSCs at time 0. The red dotted line indicates the position of hiNSCs after 96 hours. Inset scale bar = 100 μm. (C) Number of hiNSCs that showed migration over time when plated adjacent to nothing (control), MDA-MB231-Br, or A549. ***P*<0.01 by Dunnett's post-hoc test. Data presented as mean +/− SEM. Significance values represent experimental group comparisons to controls. N = 4 for controls, N = 7 for A549-GFP-NLuc, and N = 6 for MDA-MB231-Br-GFP-NLuc. (D) Movement plots of hiNSCs movement when plated opposite nothing (control), A549, or MDA-MB231-Br. Each line indicates an individual cell's movement. (E) Violin plot indicating directionality of hiNSC movement toward nothing (control), A549, or MDA-MB231-Br. *****P*<0.0001 by Dunnett's post-hoc test. (F) Violin plot indicating final displacement of hiNSC movement toward nothing (control), MDA-MB231-Br, or A549. ****P*<0.001, *****P*<0.0001 by Dunnett's post-hoc test with mean indicated by the red dot and SEM indicated by the red line. Unless otherwise specified, comparisons are not significant.

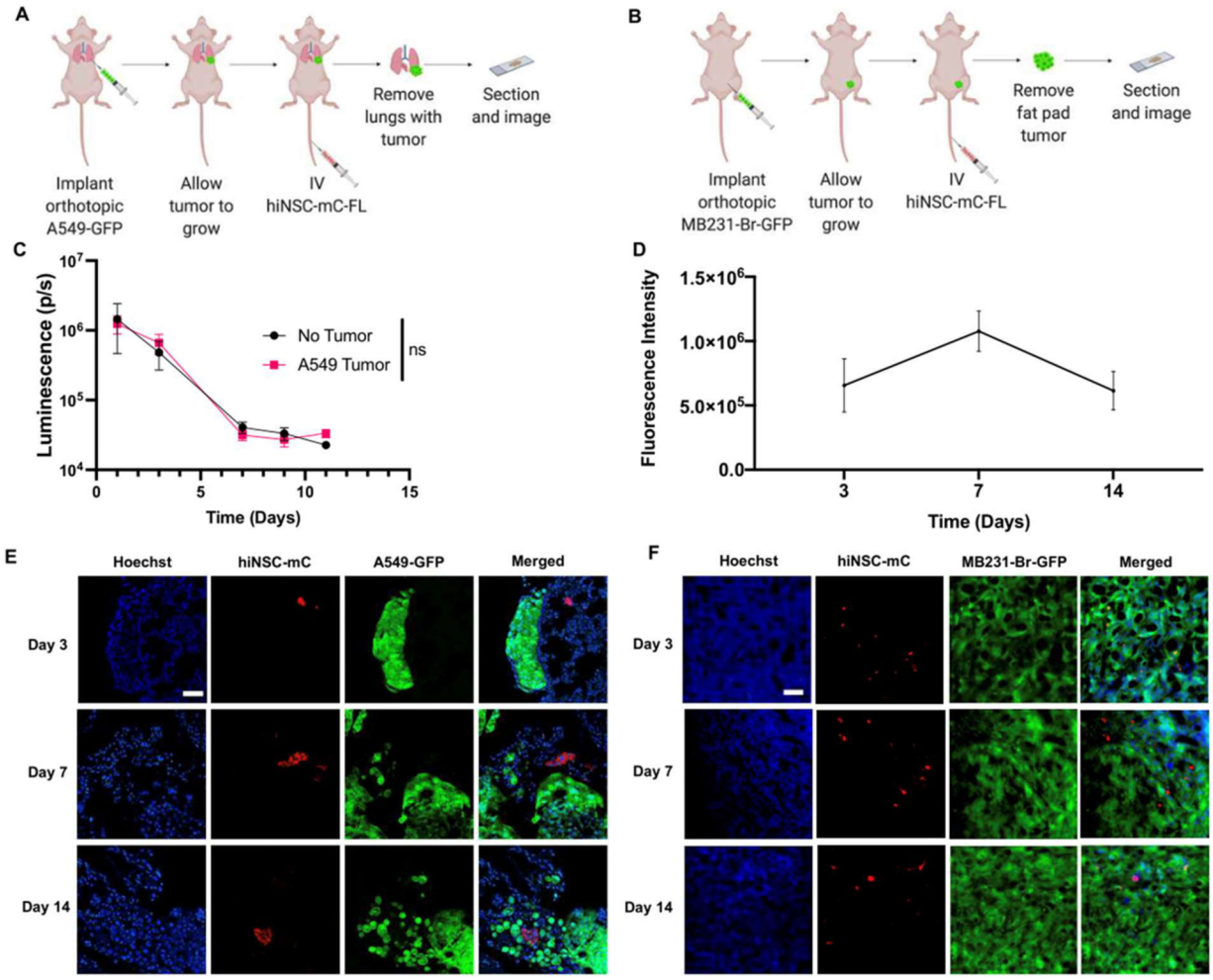

Figure 2.

Migration studies of hiNSCs *in vivo*. (A-B) Schematic of *in vivo* workflow, where mice are implanted with tumors, infused with hiNSCs intravenously, and tumors are removed and sectioned for analysis. (C) Bioluminescence signal from hiNSC-mC-FLuc cells in the thoraces of mice with (N = 10) and without (N = 5) A549-GFP tumors. Multiple unpaired t-tests without correction for multiple comparisons were used to determine significance. Mean luminescent background was 8.11×10^4 p/s. (D) hiNSC-mC-FLuc fluorescence intensity in MDA-MB231-Br-GFP fat pad tumor sections. N = 3. (E) Fluorescent images of sections of lungs with A549-GFP tumors. (F) Fluorescent images of sections of MDA-MB231-Br-GFP tumors. Scale bar = 50 μm. Data presented as mean +/− SEM.

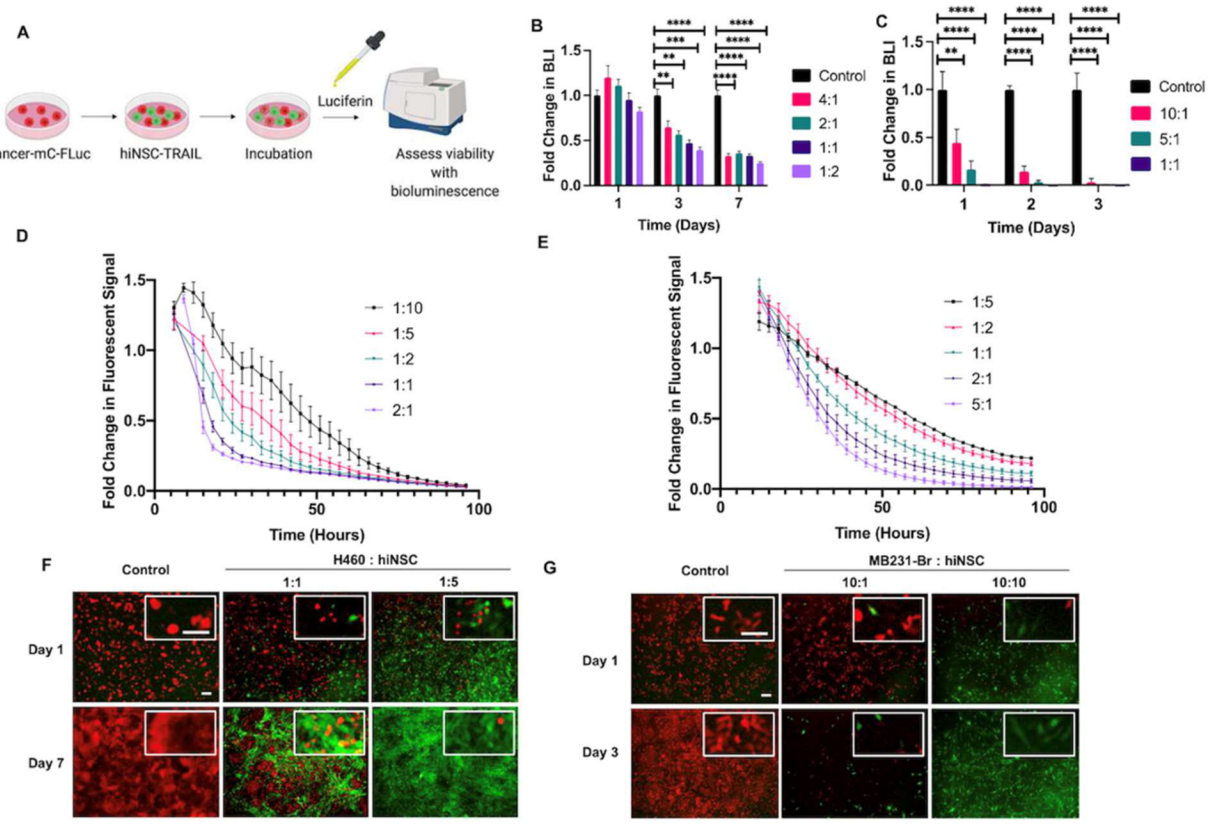

Figure 3.

hiNSC *in vitro* killing against H460 and MDA-MB231-Br. (A) Schematic of workflow to assess viability of mC-FLuc cancer cells when co-cultured with hiNSC-TRAIL cells. (B) Fold change in luminescent signal of H460-mC-FLuc when exposed to different ratios of H460: hiNSC-TRAIL over 7 days, compared to each day's tumor-only signal. ***P*<0.01, ****P*<0.001, *****P*<0.0001 by one-way ANOVA, followed by Dunnett's post-hoc test. N = 12 for control; N = 4 for all remaining groups. Unless otherwise specified, comparisons are not significant. (C) Fold change in luminescent signal of MDA-MB231-Br-mC-FLuc when exposed to different ratios of MDA-MB231-Br: hiNSC-TRAIL over 3 days, compared to each day's tumor-only signal. *****P*<0.0001 by Dunnett's post-hoc test. N = 8. (D) Kinetic killing assay of H460 cells co-cultured with varying ratios of H460: hiNSC-TRAIL cells. N = 4. (E) Kinetic killing assay of MDA-MB231-Br cells co-cultured with varying concentrations of varying ratios of MDA-MB231-Br: hiNSC-TRAIL cells. (F) Fluorescent images showing changes in H460-mC-FLuc survival following co-culture with different concentrations of hiNSC-TRAIL over 7 days. Scale bar = 200 μm. Inset scale bar = 100 μm. N = 4. (G) Fluorescent images showing changes in MDA-MB231-Br-mC survival following co-culture with different concentrations of hiNSC-TRAIL over 3 days. Scale bar = 200 μm. Inset scale bar = 100 μm.

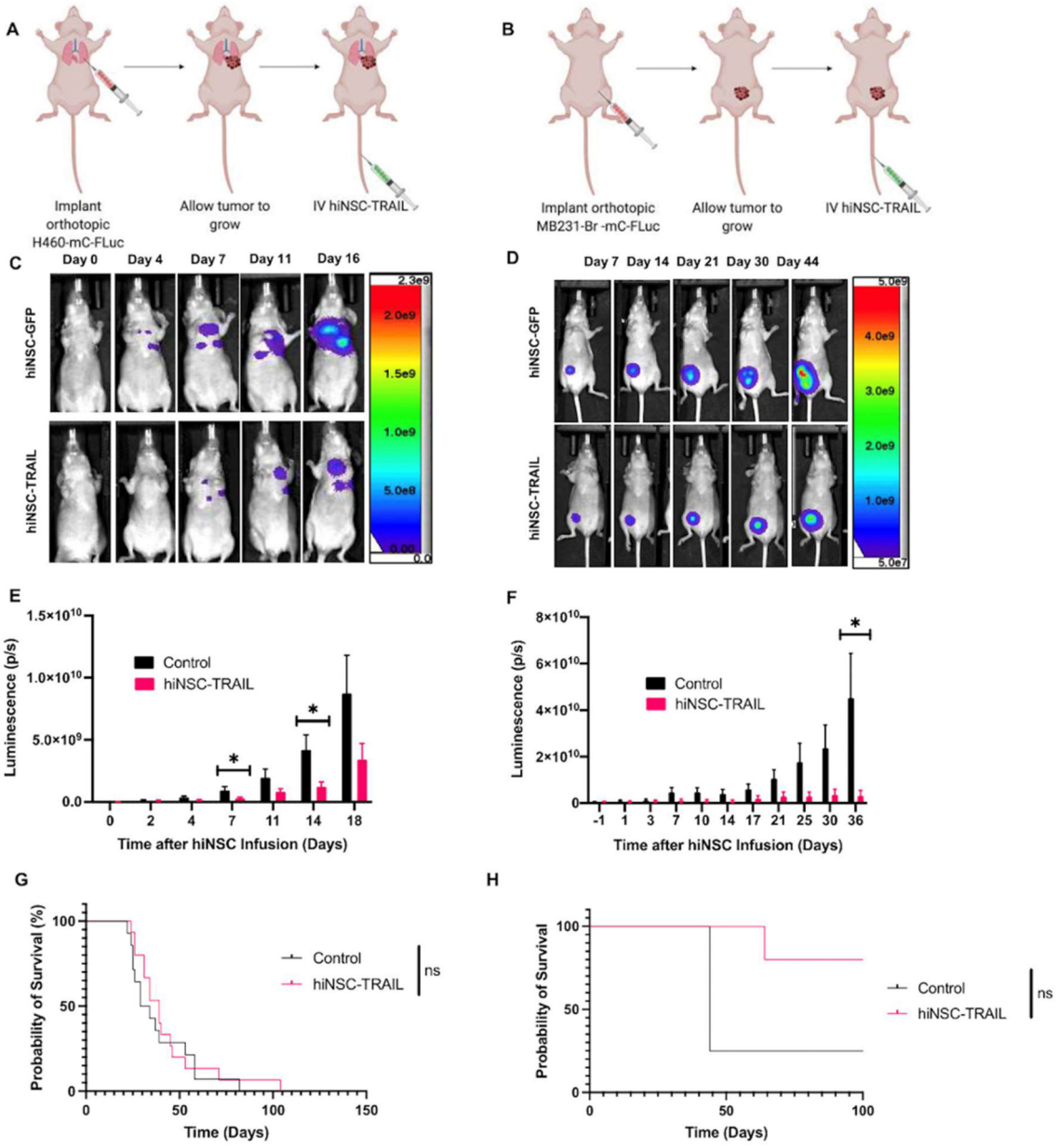

Figure 4.

Therapeutic efficacy of hiNSC-TRAIL cells against H460 and MDA-MB231-Br *in vivo*. (A-B) Schematic of workflow, establishing tumors and intravenously infusing hiNSC-TRAIL cells. (C) Representative BLI in photons/sec (p/s) for mice with H460-mC-FLuc orthotopic lung tumors treated with control (hiNSC-GFP) and therapeutic (hiNSC-TRAIL) cells. (D) Representative BLI for mice with MDA-MB231-Br-mC-FLuc fat pad tumors infused with hiNSC-GFP or therapeutic hiNSC-TRAIL cells. (E) Mean H460-mC-FLuc BLI in mice with lung tumors treated with control (hiNSC-GFP) and therapeutic (hiNSC-TRAIL) cells. N = 15 for controls, and N = 16 for mice treated with hiNSC-TRAIL. *P<0.05 by the unpaired multiple t-test without correction for multiple comparisons. (F) Mean MDA-MB231-Br BLI in mice infused with hiNSC-GFP or therapeutic hiNSC-TRAIL cells. N = 4 for control

mice, and N = 5 for mice treated with hiNSC-TRAIL. *P<0.05 by the unpaired multiple t-test without correction for multiple comparisons. Unless otherwise specified, comparisons are not significant. Data presented as mean +/− SEM. Survival curve for mice with (G) H460-mC-FLuc orthotopic tumors or (H) MDA-MB231-Br tumors treated with control or therapeutic hiNSC-TRAIL cells.

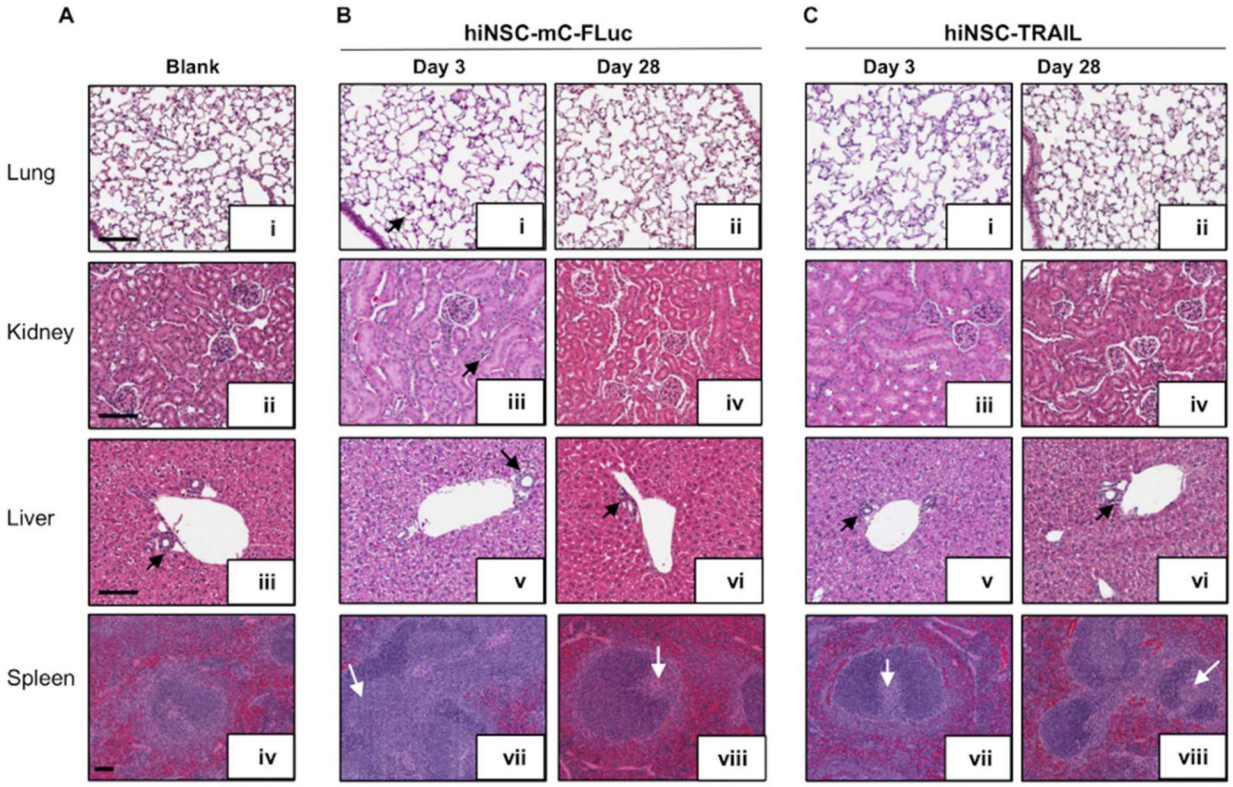

Figure 5.

Safety of intravenously-infused carrier (hiNSC-mC-FL) or carrier + drug (hiNSC-TRAIL). H&E staining of lungs (Ai, Bi, Bii, Ci, Cii), kidneys (Aii, Biii, Biv, Ciii, Civ), livers (Aiii, Bv, Bvi, Cv, Cvi), and spleens (Aiv, Bvii, Bviii, Cvii, Cviii) of (A) non-tumor bearing, non-infused mice and (B) non-tumor bearing mice 3 and 28 days after infusion of 1×10^6 hiNSC-mC-FLuc cells or (C) 1×10^6 hiNSC-TRAIL cells. The arrow in (Bi) indicates scattered cell clusters within the alveolar septal walls. Minor interstitial nephritis is indicated by arrows in (Biii). Lymphocytic infiltration is observed in (Aiii, Bv, Bvi, Cv, Cvi). Arrows in (Bvii, Bviii, Cvii, Cviii) indicate active germinal centers. Inset scale bar = 100 μm.

Table 1.

Hematology and clinical chemistry values after hiNSC-mC-FLuc and hiNSC-TRAIL infusion

				hiNSC-mC-FLuc								hiNSC-TRAIL							
	Blank			Day 3		Day 7		Day 14		Day 28		Day 3		Day 7		Day 14		Day 28	
	Mean	Low	High	Mean	SEM	Mean	SEM	Mean	SEM	Mean	SEM	Mean	SEM	Mean	SEM	Mean	SEM	Mean	SEM
Hematology																			
Red blood cells (10^6/μl)	8.56	6.11	9.53	9.2	0.1	8.78	0.19	8.49	0.09	9.68	0.16	9.28	0.18	8.83	0.32	8.27	0.47	9.05	0.24
White blood cells (10^3/μl)	2.64	0.42	7.49	0.77	0.3	0.57	0.22	1.58	0.51	6.62	1.07	6.31	1.13	3.84	0.89	1.77	0.3	1.01	0.12
Neutrophils (%)	36.12	22.9	60.5	42.73	7.2	42.1	5.47	22.05	3.35	30.2	7.14	18.43	2.81	40.13	7.31	41.1	7.19	42.3	4
Lymphocytes (%)	58.75	37.3	73.6	54.4	7.96	53.17	5.93	74.85	3.65	66.53	7.12	78.27	2.99	52.4	7.87	52.9	6.26	52.98	4.68
Monocytes (%)	2.89	0.5	14.3	2.43	0.96	3.37	1.81	1.9	0	1.23	0.13	1.57	0.13	5.5	1.06	4.55	1.85	2.8	0.64
Eosinophils (%)	1.86	0.8	2.8	0.3	0.3	0.7	0.7	0.5	0.5	1.95	0.23	1.7	0.35	1.7	0.25	1.25	0.3	1.73	0.38
Clinical Chemistry																			
Albumin (g/dL)	2.9	2.2	3.2	3.08	0.09	2.9	0.06	2.35	0.55	3.05	0.06	3.03	0.03	2.98	0.11	2.93	0.03	2.88	0.08
BUN (mg/dL)	19.95	15	26	24	1	20	1	20.5	1.5	19.75	1.18	12.75	0.48	23.5	1.94	25	0.71	16.5	0.96
Creatinine (mg/dL)	0.32	0.17	0.5	1.18	0.07	1.21	0.29	1.08	0.07	0.33	0.02	0.29	0.04	0.29	0.03	0.1	0.03	0.34	0.03
ALT (U/L)	19.5	11	38	7.75	2.17	9.33	2.33	11.5	0.5	12.75	2.06	14.25	3.28	26.25	3.45	16.75	0.63	20.75	1.11
AST (U/L)	87.5	39	302	155.25	49	100.67	12.91	169	96	48.25	3.33	110.75	42.85	100.75	3.01	64.75	2.5	170.25	10.42
ALP (U/L)	148.95	73	255	71	14.94	79.33	5.36	68.5	12.5	64.75	5.57	160.25	24.5	134.75	12.86	81.75	1.75	98.75	11.28